Eur. Phys. J. B **4**, 379–386 (1998)

THE EUROPEAN PHYSICAL JOURNAL B

II. Recirculation flow induced by a bubble stream rising in a viscous liquid

P. Snabre[a] and F. Magnifotcham

Institut de Science et de génie des matériaux et procédés[b], BP 5, 66125 Font-Romeu, France

Received: 23 July 1997 / Revised: 19 December 1997 / Accepted: 11 May 1998

Abstract. The recirculation flow induced by the rising motion of a bubble stream in a viscous fluid within an open-top rectangular enclosure is studied. The three-dimensional volume averaged conservation equations are solved by a control-volume method using a hybrid finite differencing scheme to describe the liquid phase hydrodynamics. The momentum exhange between the bubbles and the liquid phase is modeled with a source term equals to the volumetric buoyancy force acting on the gas in the bubble stream. The volumetric buoyancy force accounts for in line interactions between bubbles through the average gas volume fraction in the gas liquid column which depends on the size and the rising velocity of bubbles. The fluid flow within an open-top rectangular enclosure is further investigated by particle image velocimetry for a bubble stream rising in a water-glycerol solution. The measured fluid velocities in a vertical plane are compared with the predictions of the numerical model over a wide range of fluid viscosity (43 mPa s-800 mPa s) and gas flow rates. Finally, the recirculation flows resulting from the interaction of two neighbouring vertical bubble streams are studied.

PACS. 47.55.-t Nonhomogeneous flows – 47.55.Dz Drops and bubbles – 47.80.+v Instrumentation for fluid dynamics

Introduction

Air bubblers have been widely used in glass and metal industries to enhance the convective mixing of the molten glass or metal and improve uniformity and product quality. In glass manufacture, the rise of bubbles generated at the tank bottom further reinforces the upward current at the thermal hot spot and levels the temperature field [1–3]. When using rows of bubblers, the distance between adjacent bubble streams and the distance from the sidewalls strongly influence the efficiency of both momentum and thermal transport processes. However, a too strong bubbling may lead to production problems related to fluid contamination arising from the formation of a surface foam or the accelerated attack of the tank bottom.

The rising bubbles act as exterior shear forces on the surrounding fluid and induce a liquid recirculation. Empirical relations were proposed to estimate the momentum exchange coefficient between bubble stream and the liquid [4]. A slip velocity between air bubbles and the surrounding fluid is generally introduced to describe the effect of bubbling on the transport processes. However, the coupling between the bubble stream and the fluid phase often ignores in line hydrodynamic interactions which strongly influence both the rising velocity of bubbles and the momentum exchange.

A companion paper [5] was dedicated to an experimental and theoretical study of bubble size and rise velocity of a bubble stream in a viscous liquid. We have proposed a physical model to estimate the rising velocity of in line interacting bubbles and the gas volume fraction in the bubble stream. The volumetric buoyancy force determines the momentum exchange and accounts for in line interactions between bubbles through the average gas volume fraction in the bubble stream depending on bubble size and rising velocity.

Earlier and more recently, various numerical models [6–8] have been developed for solving fluid flow and heat transfer problems in recirculation flows. All the above mentioned numerical models are based on the solution of the finite difference form of the volume averaged conservation equations. However, before numerical modelling can be used with confidence to industrial problems, model predictions must be verified by independent experimental data.

We present a three-dimensional numerical model to predict the recirculation flow induced by a rising bubble stream in a viscous fluid within an open-top rectangular enclosure. The liquid phase hydrodynamics is modelled through a control volume approach by solving the volume averaged mass and momentum conservation equations. The SIMPLE (Semi-Implicit Method for Pressure Linked Equations) algorithm of Patankar [7,9] is used to solve finite difference equations. The control volume

[a] e-mail: snabre@imp-odeillo.fr
[b] UPR 8521.

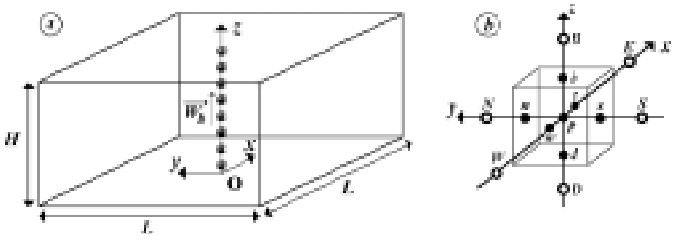

Fig. 1. Schematic representation of a single bubble stream within an open-top rectangular enclosure (a) and an elementary control volume (b).

approach highlights the physical processes and the SIMPLE algorithm using pressure and velocities as the main flow variables is powerful from the convergence rate standpoint [7].

In a second section, a particle image velocimetry (PIV) technique is used in conjunction with advanced image processing techniques to measure local flow properties in a vertical plane [10,11]. Velocity data for the upward bubble stream and the surrounding liquid within an open-top rectangular enclosure are presented and compared to the predictions of the numerical model.

1 Volume averaged conservation equations

The system under consideration is shown schematically in Figure 1a. Bubbles are generated in a stream from a nozzle submerged in a viscous Newtonian liquid. Temperature and density of the liquid phase are assumed to be uniform within an open-top rectangular enclosure (height H and width L large compared to the bubble diameter d). In the case of a single bubble stream, the nozzle is located at the centre of the tank bottom face (point O taken as the origin of the coordinate system, Fig. 1).

Under isothermal conditions, the liquid flow is governed by the volume averaged continuity and momentum equations. Assuming incompressible fluid and neglecting the transient terms, the volume averaged conservation equations can be expressed in vector notation as:

• Continuity

$$\nabla \cdot ((1-\varepsilon)\rho \mathbf{U}) = 0 \tag{1}$$

• Momentum

$$((1-\varepsilon)\rho \mathbf{U}\cdot\nabla)\mathbf{U} = -(1-\varepsilon)\nabla P + \nabla\cdot[(1-\varepsilon)\eta(\nabla\cdot\mathbf{U})] + (1-\varepsilon)\rho\mathbf{g} + \boldsymbol{\Psi}$$

where $\mathbf{U}(u,v,w)$ is the liquid phase velocity vector in the Cartesian coordinates (x,y,z), $\mathbf{g}$ the gravity acceleration, ε the gas volume fraction, ρ the liquid density, η the liquid viscosity and P the fluid pressure.

The coupling between the gas and the liquid phase appears through the vector $\boldsymbol{\Psi}$ which represents the volume averaged momentum exchange between the bubbles and the liquid phase. Neglecting the transverse components, the momentum exchange vector equals the volume averaged buoyancy force acting on the gas [12]:

$$\begin{aligned} &\boldsymbol{\Psi} = -\varepsilon\langle\rho\rangle\mathbf{g} \quad \text{for} \quad r \le d/2 \quad \text{and} \quad 0 \le z \le H \\ &\boldsymbol{\Psi} = \mathbf{0} \quad \text{for} \quad r \ge d/2 \end{aligned} \tag{2}$$

where $\langle\rho\rangle = (1-\varepsilon)\rho$ is the volume averaged density of the gas liquid column, r the radial distance from the bubble stream axis and d the bubble diameter. The momentum conservation equation then takes the fom:

$$(\rho\mathbf{U}\cdot\nabla)\mathbf{U} = -\nabla P + \nabla\cdot[\eta(\nabla\cdot\mathbf{U})] + \rho\mathbf{g} + \mathbf{S}_b \tag{3}$$

with

$$\mathbf{S}_b = -\rho\varepsilon\mathbf{g}$$

where the momentum source vector $\mathbf{S}_b = -\rho\varepsilon\mathbf{g}$ represents the volumetric buoyancy force acting on the liquid phase. Considering the number $N = \varepsilon(\pi d^2/4)H/V$ of bubbles in the gas-liquid column, the net average bubbling force $\mathbf{F}_b$ then reduces to the liquid weight displaced by air bubbles within the stream [5]:

$$\mathbf{F}_b = \frac{\pi d^2 H}{4}\mathbf{S}_b = -\rho N V \mathbf{g} \tag{4}$$

where V is the bubble volume. The volume averaged gas volume fraction $\varepsilon = Qd/(W_b V)$ in the gas liquid column depends on the gas flow rate Q through the nozzle and the rising velocity W_b of in line interacting bubbles [5].

Neglecting the acceleration stage after bubble detachment and the drop deceleration near the liquid free surface, the bubble size and rise velocity of a bubble stream in an unbounded viscous liquid were determined in a companion paper through semi empirical models and physical considerations [5]:

$$\frac{\pi}{3}d^3\rho g = \left(\frac{81 C_d^*}{16} + 9\alpha\right)\frac{\rho Q^2}{\pi d^2} + \pi d_a \sigma \tag{5}$$

with

$$C_d^* = \frac{24}{Re} + 1,\ Re = \frac{\rho W d}{\eta} \text{ and } W = \frac{3dQ}{4V},$$

$$W_b^2 = \frac{2dg(1+\varepsilon)}{C_d} \tag{6}$$

with

$$\varepsilon = \frac{Qd}{W_b V} \text{ and } C_d = \frac{16}{Re} + 1 = \frac{16\rho W_b d}{\eta} + 1$$

where α is an inertial parameter, d_a the nozzle diameter, σ the surface tension of the liquid and W the average velocity of bubble expansion [5]. The momentum source vector $\mathbf{S}_b$ is calculated from the relation (3) with an average gas volume fraction $\varepsilon(V, W_b)$ derived from the equations (5, 6).

Concerning the boundary conditions, we assume continuity of the volume averaged liquid velocity and viscous stress at the frontier between the bubble stream and the

surrounding fluid. Along the vertical axis of the bubble stream, the viscous stress in horizontal planes further cancel. The fluid from the sides and from the bottom is surrounded by walls where the boundary conditions for velocities are of "no-slip" type. The top surface of the liquid is exposed to the ambient air. Neglecting viscous stresses in the air and surface tension effects, the boundary conditions at the free surface are:

$$w(H) = 0 \text{ and } \left.\frac{\partial u}{\partial z}\right|_{z=H} = \left.\frac{\partial v}{\partial z}\right|_{z=H} = 0. \qquad (7)$$

Since no fluid velocity is imposed near the bubble stream and only continuity of the volume averaged liquid velocity is assumed, the liquid-bubble interaction is superimposed on the liquid velocity field and then the model describes the coupling between the gas-liquid column and the nearby boundary layer.

However, the physical model used to estimate the gas volume fraction in the bubble stream ignores the effect of liquid recirculation on the bubble stream dynamics. In a liquid bath of finite extent, the large scale recirculation flow may influence the bubbling growth and the rising velocity of bubbles. In this work, the distance between the bubble stream and sidewalls (or between neighbouring bubble streams) is larger than the thickness $\delta \approx [\eta H/(\rho W_b)]^{1/2}$ of the viscous boundary layer (0.4 cm $< \delta <$ 3 cm with 0.043 Pa s $< \eta <$ 0.8 Pa s, 5 cm/s $< W_b <$ 40 cm/s, $\rho = 1250$ kg/m^3 and $H = 8$ cm) and therefore we may neglect the effect of the recirculation flow on the bubble stream dynamics [5].

2 Three-dimensional numerical model

A computer model based on a control-volume method using hybrid finite difference scheme was developed to solve the conservation equations with a momentum source vector $\mathbf{S}_b(0, 0, S_{bz})$ given by equation (3). The calculation domain is split up in control volumes as illustrated in Figure 1b with a spatial resolution smaller than the bubble size in the gas-liquid column. We may write the conservation equations (1, 3) into a general equation of the form:

$$\nabla \cdot (\rho\phi\mathbf{U}) = \nabla \cdot (\Gamma_\phi \nabla\phi) + \mathbf{S}_\phi \qquad (8)$$

where ϕ, Γ_ϕ and $\mathbf{S}_\phi$ denote the dependent variables, the diffusion coefficient and the source term respectively (Tab. 1).

Application of the Gauss divergence theorem to equation (8) yields:

$$\int_{\sigma_c} (\rho\mathbf{U}\phi - \Gamma_\phi \nabla_\phi) \cdot \mathbf{n} d\sigma_c = \int_{V_c} \mathbf{S}_\phi dV_c \qquad (9)$$

where σ_c is the surface area and V_c the volume of a finite elementary cell. The left hand term represents the convection and diffusion fluxes through the six faces (w, e, s, n, b, d) of the control volume (Fig. 1b) and the right term is the source flux at the centre node P of the control volume. The combined convection diffusion fluxes across the faces of a control volume are evaluated using the hybrid finite difference scheme [7,9]. Finite difference approximations for partial derivatives and integral (9) then yields an algebraic equation of the form:

$$A_P\phi_P = A_W\phi_W + A_E\phi_E + A_N\phi_N + A_S\phi_S + A_B\phi_B + A_D\phi_D + S_P \qquad (10)$$

for each volume control in the calculation domain where the subscript (W, E, N, S, B, D) denote the neighbouring nodes surrounding node P (Fig. 1b). The above equation involves the values of variable ϕ and source term $\mathbf{S}_\phi$ at node P and neighbouring nodes. The coefficients A resulting from combined convection/diffusion fluxes across the faces of the control volume are detailed in [7]. The value of the dependent variables (u, v, w) are considered either at the centre node P or at the faces of the control volume [7].

Table 1. Dependent variables ϕ, diffusion coefficient Γ_ϕ and source term $\mathbf{S}_\phi$ in equation (8) for each of the volume averaged conservation equations.

	ϕ	Γ_ϕ	$\mathbf{S}_\phi$
Continuity	1	0	0
x-momentum	u	η	$-\partial P/\partial x$
y-momentum	v	η	$-\partial P/\partial y$
z-momentum	w	η	$-\rho g + S_{bz} - \partial P/\partial z$

However, the presence of the pressure gradient in the volume averaged momentum equations requires the prediction of the pressure field. The main difficulty arises from the lack of an explicit equation for the pressure field. Fortunately, a pressure equation is obtained by substituting the algebraic form (10) of the momentum equation into the discretized continuity equation.

Since the coefficient A of the algebraic equations are functions of the dependent variable ϕ, the solution procedure is an iterative process based on the SIMPLE method [7,9]. In summary, an initial guessed pressure field is used to compute the velocity field (u, v, w) from momentum equations. Since the calculated velocities do not satisfy the mass conservation, pressure and continuity equations are then solved to yield corrections to the pressure and the velocity field. The tri-diagonal matrix algorithm (TDMA) [7] is used to solve the system of algebraic equations.

The above steps are repeated until the change in the velocity components is less than 3%. Furthermore, the sum of the residual mass errors over the entire calculation domain to the fluid mass in the tank must be less than 10^{-6} as a second convergence criterion. An underrelaxation method is used for optimum ultimate convergence of the iteration cycle.

The solution procedure converges to acceptable accurate result for a $40 \times 40 \times 15$ non uniform grid with smaller control volumes in the bubble stream region (Fig. 2). The calculations performed on a computer HP 9000 grade 730

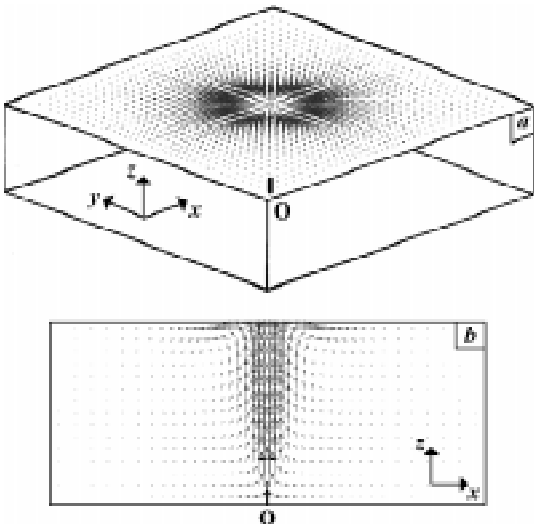

Fig. 2. Liquid velocity field at the liquid free surface $z = H$ (a) or in the vertical plane $y = 0$ (b) calculated from the three-dimensional mathematical model for a single bubble stream.

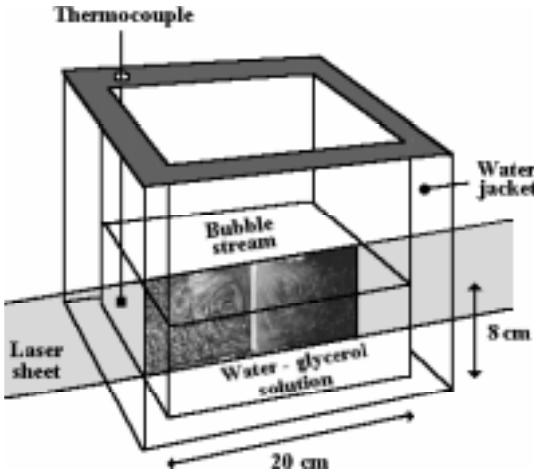

Fig. 3. Experimental set-up to visualise the full field flow pattern by illuminating a single rising bubble stream in a water-glycerol solution with a thin sheet of light.

with 70 Mb memory and 70 mips frequency take one two twenty minutes for a maximum iteration number of about 150.

3 Experimental set-up

The recirculation flow induced by one or two bubble streams rising in a viscous liquid were studied experimentally. Experiments were performed under constant temperature conditions in a glass tank of 20 cm × 20 cm internal cross section and 20 cm height (Fig. 3). The tank was filled with a water-glycerol solution up to a height of 8 cm. The viscosity of the Newtonian liquid ranging from 43 mPa s up to 800 mPa s was measured with a Couette rheometer (Low shear 30, Contraves).

The liquid temperature was maintained to 20 °C with a water jacket surrounding the tank sidewalls and controlled with ± 0.1 °C accuracy. Air bubble streams were generated from a steel tube of inner diameter $d_a = 0.6$ mm with gas flow rates ranging from 0.05 l/mn up to 0.5 l/mn measured with a flowmeter.

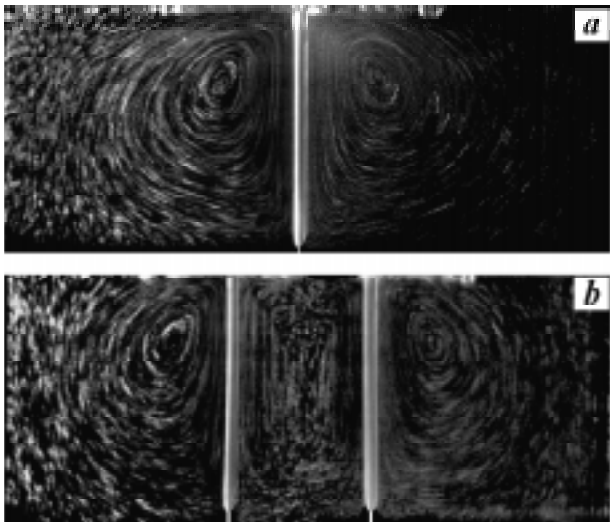

Fig. 4. Visualisation of the flow induced by a single bubble stream (a) or two bubble streams (b) rising in a water-glycerol solution of viscosity $\eta = 105$ mPa s (gas flow rate $Q = 0.048$ l/mn, liquid depth $H = 8$ cm).

Particle image velocimetry is a flow visualization technique which allows non invasive velocity measurements over a full flow field [10,11]. The particle image velocimetry system developed in the present work uses a 4 W argon ion laser (American laser). Optical accessories consisting of a long fiber optic cable, a focusing lens and a rotating polygonal mirror generate a vertical pulsed laser sheet of 0.3 mm thickness and 12 cm width at the camera view plane (Fig. 3). Micron sized particles were used as tracers to visualise the movement of the liquid phase. Air bubbles generated at the nozzle served as natural seeding for the gaseous component.

The motion of particles and bubbles within the vertical light plane passing through the bubble stream was recorded by a 512 × 512 pixel resolution CCD camera (Sony XC77RR) with 256 grey level resolution (Fig. 4). The CCD camera operates in conjunction with a Mattrox PIP 1024 imaging unit and a PC compatible for the digitisation and storage of image data. The camera is further equipped with a variable electronic shutter controlled in real time through TTL signals delivered by a DT2817 card (Data Translation) located in the computer. The calibration factor for the field of view and any magnification was measured prior to frame record.

Typically, a succession of 4 frames was recorded in non interlaced mode for a better contrast. The camera shutter speed 50 Hz $< \omega < 10^4$ Hz and the time delay $dt \leq 0.02$ s between frames were adjusted to improve image quality and obtain detectable seed displacement. Figure 5 shows a 4-frame overlay depicting the seed spots motion near the bubble stream for a shutter speed $\omega = 1360$ Hz and a time delay $dt = 0.02$ s between successive image frames.

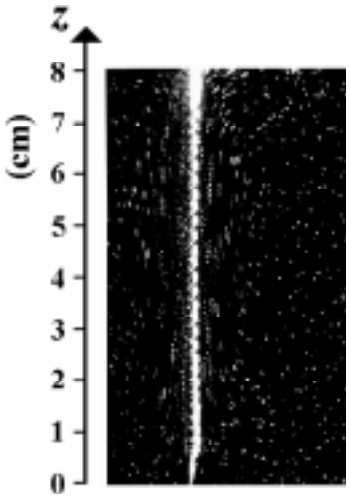

Fig. 5. Overlay of 4 binary frames showing the induced particle motion near a single bubble stream rising in a water-glycerol solution of viscosity $\eta = 164$ mPa s (gas flow rate $Q = 0.048$ l/mn, liquid height $H = 8$ cm, delay time between successive frames $dt = 0.02$ s, shutter speed $\omega = 1360$ Hz).

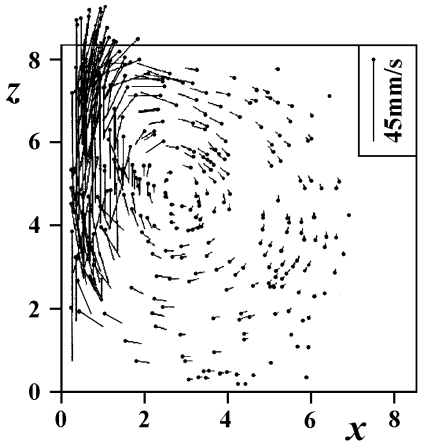

Fig. 6. Particle velocity vectors resulting from the rising of a single bubble stream in a water-glycerol solution of viscosity $\eta = 164$ mPa s (gas flow rate $Q = 0.048$ l/mn and liquid height $H = 8$ cm)

When increasing the interval time dt between frames, the particle motion at larger distances from the bubble stream may be evaluated. Several image data sets of the flow were recorded and subsequently analysed to determine the full-field velocity profile.

Specific numerical algorithms were developed to compute seed spots displacement between successive image frames. A program first performs grey level thresholding to improve image quality. The next step is to label seed spots and determine the spot correspondence between image pairs. A spatial point to point correlation routine first proposed by Yamamoto [13] was implemented to determine velocity vectors for each seed displacement at the exact spatial position of the seed spot within the image frame. The degree of correspondence between seeds in separate image frames is measured by calculating a cross correlation coefficient for each possible seed pair within a subregion [14]. However, some degradation in the seed spot correspondence is observed in three-dimensional flows since some seeds may leave the light plane. Therefore, we only consider seed spots with a cross correlation coefficient above a specified limiting value [13,14]. From the time interval dt between image pairs and the calculation of tracer displacement, the fluid velocity field in the light plane is then determined with $\pm$ 3% accuracy (Fig. 6).

4 Experimental results

4.1 Single vertical bubble stream

A bubble stream generated in a viscous fluid induces an upward flow and a large scale recirculation flow. The four frame overlay presented in Figure 7 shows the rotating current near the bubble stream in the vertical plane $y = 0$. We define the centre point $C(x_c, z_c)$ of the recirculation

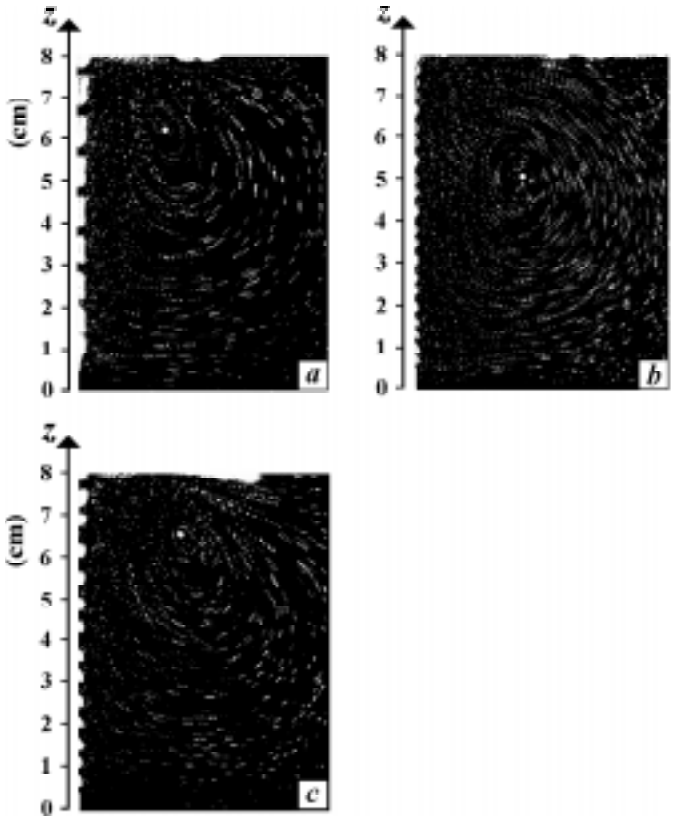

Fig. 7. Overlay of 4 binary frames showing the recirculation flow induced by a single rising bubble stream in a water glycerol solution (liquid height $H = 8$ cm, shutter speed $\omega = 1360$ Hz). The white circle indicates the centre of the recirculation flow. (a) $\eta = 43$ mPa s, $Q = 0.048$ l/mn, $dt = 0.2$ s, (b) $\eta = 164$ mPa s, $Q = 0.048$ l/mn, $dt = 0.2$ s, (c) $\eta = 43$ mPa s, $Q = 0.25$ l/mn, $dt = 0.1$ s.

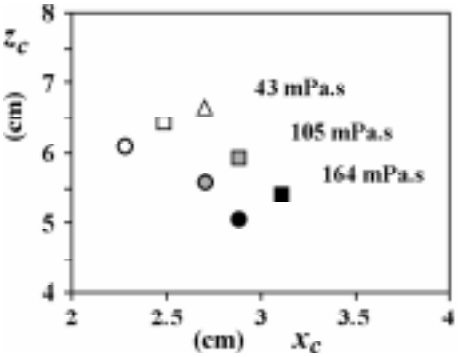

Fig. 8. Space coordinates $(x_c,\ z_c)$ of the recirculation flow center as a function of gas flow rate and liquid viscosity. The length x_c is the distance from the single bubble stream axis in the vertical plane $y = 0$ and z_c the distance from the tank bottom. (○) $Q = 0.048$ l/mn, (□) $Q = 0.1$ l/mn, (△) $Q = 0.25$ l/mn, $\eta = 43$ mPa s for white symbols, $\eta = 105$ mPa s for grey symbols and $\eta = 164$ mPa s for black symbols.

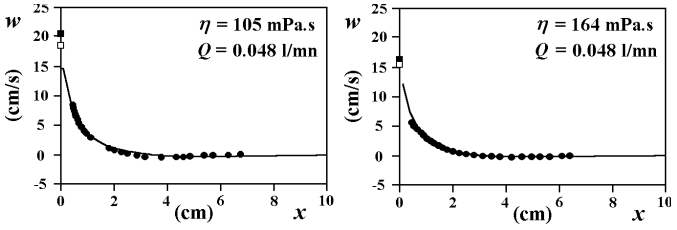

Fig. 9. Vertical liquid velocity component $w(x)$ *versus* the distance x from the single bubble stream in the vertical plane $y = 0$ at the height $z = z_c$ for fluid viscosity $\eta = 105$ mPa s (left figure) and $\eta = 164$ mPa s (right figure). Gas flow rate $Q = 0.048$ l/mn and liquid height $H = 8$ cm. The black circles represent the experimental liquid velocity data and the solid line the predictions of the numerical model. (■) Measured bubble rise velocity. (□) Calculated bubble rise velocity from equations (5, 6).

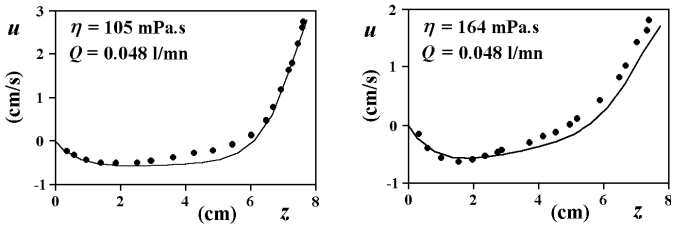

Fig. 10. Horizontal liquid velocity component $u(z)$ *versus* the height z from the tank bottom in the vertical plane $y = 0$ at the distance $x = x_c$ from the single bubble stream axis for fluid viscosity $\eta = 105$ mPa s (left figure) and $\eta = 164$ mPa s (right figure). Gas flow rate $Q = 0.048$ l/mn and liquid height $H = 8$ cm. The black circles represent the experimental liquid velocity data and the solid line the predictions of the numerical model.

flow where the fluid velocity cancels in the vertical plane $y = 0$. Under constant gas flow rate conditions, the centre point C moves away from the liquid free surface and from the bubble stream axis when increasing the fluid viscosity from 43 mPa s to 164 mPa s (white circles in Figs. 7a and 7b). A high viscosity enhances the momentum diffusion in the fluid phase and the space extent of the recirculation zone. On the other hand, the centre point C moves closer to the free surface at high gas flow rates (Figs. 7a and 7c) because inertial effects have a more pronounced influence in the momentum equations. The viscosity and gas flow rate dependence of the centre point coordinates $x_c(Q, \eta)$ and $z_c(Q, \eta)$ in the vertical plane $y = 0$ are shown in Figure 8.

The z-component $w(x)$ and x-component $u(z)$ of the liquid velocity were derived from the cross correlation analysis of successive image pairs. Figure 9 shows the x variation of the vertical liquid velocity $w(x)$ at the height $z = z_c$. The streamlines are nearly parallel to the vertical axis near the bubble stream. The vertical velocity component $w(x)$ steeply decreases over a distance $x_c/2$ scaling as the thickness $\delta \approx [\eta H/(\rho W_b)]^{1/2}$ of the vertical boundary layer and increasing with the liquid viscosity ($\delta \approx 1$ cm for $\eta = 164$ mPa s, $H = 8$ cm, $\rho = 1250$ kg/m^3 and $W_b \approx 15$ cm/s) (Fig. 9).

At the distance $x = x_c$ from the bubble stream axis, the horizontal velocity component $u(z)$ displays smaller values along the vertical z axis except near the liquid free surface where the fluid velocity takes a maximum value u^* (Fig. 10). The velocity $u^*(x, H)$ of the liquid free surface in the vertical plane $y = 0$ increases with the rising velocity W_b of bubbles and approximately scales as $W_b d/x$. The flow near the free surface presents a boundary layer character with streamlines nearly parallel to the horizontal plane and relatively steep velocity gradients. In the vertical plane $y = 0$, the thickness of the horizontal boundary layer near the liquid free surface then scales as $[\eta x/\rho u^*)]^{1/2} \approx x[\eta/(\rho W_b d)]^{1/2}$ and increases linearly with the distance x from the bubble stream axis. The streamlines in Figure 4 indeed indicate a rapid increase of the horizontal boundary layer thickness with the distance from the bubble stream.

Figures 9 and 10 show the general agreement between experimental velocity field and predictions of the numerical model. The bubble rising velocity W_b derived from equations (3, 4) decreases with fluid viscosity in good agreement with experimental data. The vertical fluid velocity near the gas liquid column is about $3W_b/4$ (Fig. 9) which explains the empirical models based on a slip velocity to describe the momentum exchange between air bubbles and the surrounding liquid [4].

When increasing the liquid viscosity, the recirculation flow slows down within the tank (Figs. 9 and 10) because of the decrease of the average buoyancy force $S_{bz} = \rho g \varepsilon$ per unit volume acting on the gas in the bubble stream. Despite larger bubble volume, a viscosity increase lowers both the bubble frequency emission and the gas volume fraction ε in the stream [5] which reduces the momentum exchange. On the other hand, both the bubble frequency emission and gas volume fraction ε increase with gas flow rate which enhance the recirculation flow and improve the convective mixing in good agreement with theoretical results (Figs. 9 and 11).

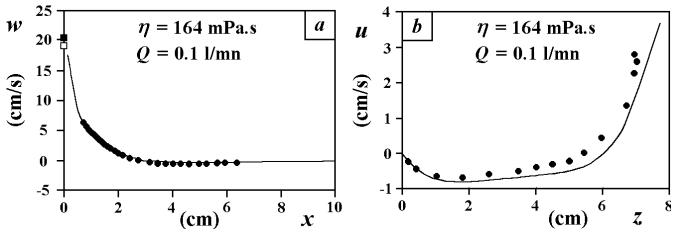

Fig. 11. Vertical liquid velocity component $w(x)$ *versus* the distance x from the single bubble stream in the vertical plane $y = 0$ at the height $z = z_c$ (a). Horizontal liquid velocity component $u(z)$ *versus* the height z from the tank bottom in the vertical plane $y = 0$ at the distance $x = x_c$ from the bubble stream axis (b). Fluid viscosity $\eta = 164$ mPa s, gas flow rate $Q = 0.1$ l/mn and liquid height $H = 8$ cm. The black circles represent the experimental liquid velocity data and the solid line the predictions of the numerical model. (■) Measured bubble rise velocity. (□) Calculated bubble rise velocity from equations (5, 6).

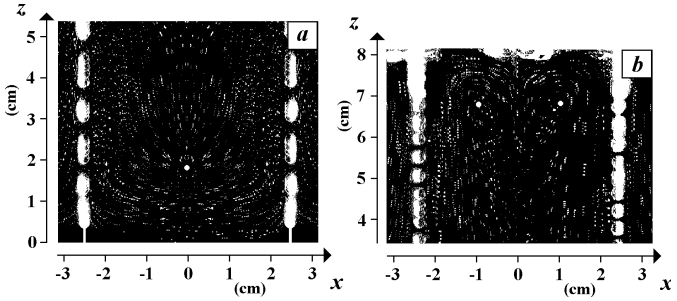

Fig. 12. Overlay of 4 binary frames showing the flow pattern between two vertical bubble streams apart from 5cm in a water glycerol solution (liquid viscosity $\eta = 105$ mPa s, gas flow rate $Q = 0.048$ l/mn, liquid height $H = 8$ cm and shutter speed $\omega = 1360$ Hz). Figures (a) and (b) respectively show the bottom and upper region of the flow. The white circles indicate either the quiescent region in (a) or the centre of the secondary flows in (b).

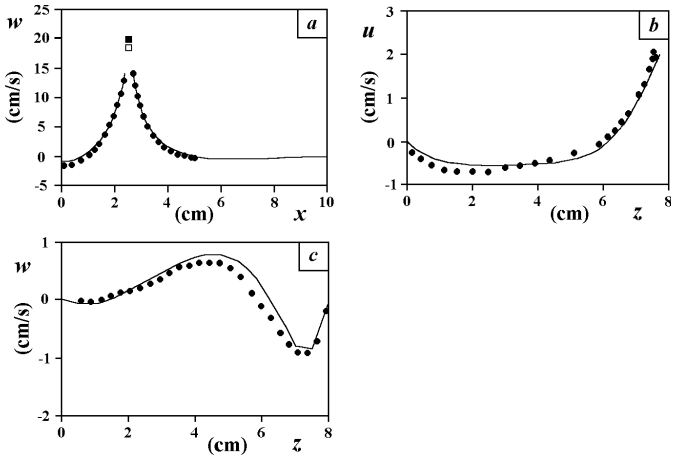

Fig. 13. Liquid flow in the vertical plane $y = 0$ induced by two bubbles streams rising in a water-glycerol solution of viscosity $\eta = 105$ mPa s (gas flow rate $Q = 0.048$ l/mn and liquid height $H = 8$ cm). Vertical liquid velocity component $w(x)$ *versus* the distance x from the bubble stream at the height $z = z_c = 6.7$ cm (a). Horizontal liquid velocity component $u(z)$ *versus* the height z from the tank bottom at the distance $x = 5$ cm (b). Vertical liquid velocity component $w(z)$ *versus* the height z from the tank bottom at the distance $x = 0$ (c). The black circles represent the experimental liquid velocity data and the solid line the predictions of the numerical model. (■) Measured bubble rise velocity. (□) Calculated bubble rise velocity from equations (5, 6).

4.2 Two vertical bubble streams

We have investigated the flow field resulting from the interaction of two bubble streams (Fig. 4b). The two nozzles are located symmetrically in the vertical plane $y = 0$ at a distance of 2.5 cm from the centre point O of the bottom wall. The separation distance of 5 cm between bubblers is larger than the thickness $\delta \approx [\eta H/(\rho W_b)]^{1/2}$ of the vertical viscous boundary layer and we may expect only small hydrodynamic perturbation of the bubble streams ($\delta \approx 0.6$ cm for $\eta = 105$ mPa s, $H = 8$ cm, $\rho = 1250$ kg/m^3 and $W_b \approx 20$ cm/s) (Fig. 9).

The large scale flow pattern in the vertical plane $y = 0$ and for $x > 2.5$ cm is remarkably close from the flow induced by a single bubbler (Fig. 13a). In the region between the two bubblers, the hydrodynamic interactions between the recirculation flows induced by each rising bubble stream results in a loss of the radial symmetry of the streamlines. One observes an upward flow from a bottom point located between the bubblers (white circle in Fig. 12a). The upward flow arises from the junction of the large scale recirculation flows in the vertical plane $x = 0$ perpendicular to the light plane.

The hydrodynamic interaction of the horizontal boundary layers generates small scale recirculation flows in the immediate vicinity of the free liquid surface (white circles in Fig. 12b). For a gas flow rate $Q = 0.048$ l/mn and a fluid viscosity $\eta = 105$ mPa s, the centre point C of the secondary recirculation flows is located at the height $z_c = 6.7$ cm and 1.4 cm from the bubble axis ($x_c = \pm 0.9$ cm).

Far from the region between bubble streams ($x > 2.5$ cm), the vertical velocity $w(x)$ at the height $z = z_c$ (Fig. 13a) and the horizontal velocity component $u(z)$ at $x = 5$ cm (Fig. 13b) display comparable variation when compared to the flow pattern for a single bubble stream (Figs. 9 and 10). The vertical velocity component $w(z)$ between bubble streams takes lower values along the vertical z axis ($w(z,\ x = 0) < 1$ cm/s, Fig. 13c) in good agreement with numerical predictions. The bottom region between bubble streams in the vertical plane $y = 0$ is nearly quiescent which strongly weakens the efficiency of the convective mixing.

4.3 Effect of a circular ring

In the companion paper [5], we have investigated the effect of a circular ring located at the emission orifice on bubble growth and rise velocity. The circular ring screens

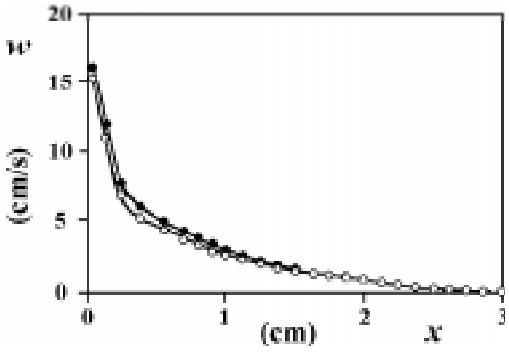

Fig. 14. Vertical liquid velocity component $w(x)$ *versus* the distance x from the single bubble stream in the vertical plane $y = 0$ at the height $z = z_c = 5$ cm in the absence (•) or in the presence (○) of a 3 cm diameter circular ring located at the emission orifice (fluid viscosity $\eta = 164$ mPa s, gas flow rate $Q = 0.048$ l/mn and liquid height $H = 8$ cm).

the large scale recirculation flow near the orifice which delays the detachment of the bubble and slightly lowers the bubble rise velocity mainly sensitive to the bubbling frequency [5]. In the same way, we have studied the liquid flow pattern induced by a single bubble stream released from a nozzle with a circular ring of 3 cm diameter. The analysis of the image frames only shows a slight decrease of the vertical velocity component $w(z)$ near the bubble stream and negligible influence of the circular ring on the large scale recirculation flow (Fig. 14). In the presence of the screening ring, the lower fluid velocity near the bubble stream mainly results from the smaller average gas volume fraction ε in the gas-liquid column which lowers the momentum exchange.

5 Conclusion

A three-dimensional numerical model based on control-volume approach and hybrid finite differencing scheme was developed with a momentum steady source term in the z-momentum equation to describe the momentum exchange between the rising bubble stream and the liquid phase within an open-top rectangular enclosure. The full-field flow in a two dimensional plane was further investigated with a particle image velocimetry system using advanced image processing. The point by point cross correlation analysis of the digitised image frames accurately yields the bubble rise velocity and the fluid velocity in the laser light plane.

The numerical model well describes the experimental flow pattern. Therefore, the theoretical expressions of the momentum source term and the gas volume fraction in the bubble stream account for in line interactions between bubbles and can be used with confidence in numerical models to describe the momentum exchange in industrial reactors involving air bubblers. However, the present model neglects the effect of the large scale recirculation flow on bubble growth and rise velocity which assumes distances between a bubble stream and sidewalls (or between neighbouring bubble streams) larger than the thickness of the viscous boundary layer.

When considering row of bubblers to improve convective mixing and quality product in chemical reactors, care must be taken to set the distance between adjacent bubblers. For distances between adjacent air bubblers larger than the thickness of the vertical boundary layer, the bottom region between bubble streams is nearly quiescent. On the other hand, smaller separation distances between air bubblers induce the formation of small extent secondary flows which promotes small scale convective mixing. However, the hydrodynamic interactions between close bubblers then may perturb the bubble growth and rise velocity.

References

1. A. Ungan, W.H. Turner, R. Viskanta, Glastech. Ber. **56K**, 125-129 (1983).
2. F. Simonis H. De Waal, R.C.G. Beerkens, *Influence of furnace design and operation parameters on the residence time distribution of glass tanks, predicted by 3-D computer simulation, XIV Int. Congr. on Glass, New Delhi*, Vol. 3 (1986) pp. 118-128.
3. W. Trier, *Glass furnaces, Design construction and operation* (Society of Glass Tech., 1987).
4. A. Ungan, R. Viskanta, J. Am. Ceram. Soc. **69**, 382-391 (1986).
5. P. Snabre, F. Magnifotcham, Eur. Phys. J. B. **4**, 369-377 (1998).
6. A.D. Gosman, M. Pun, A.K. Runchal, D.B. Spalding, M. Wolfshtein, *Heat and mass transfer in recirculating flows* (Academic Press, London and New York, 1969).
7. S.V. Patankar, *Numerical heat transfer and fluid flow* (Hemisphere Publishing Co. Mc Graw-Hill, 1980).
8. A. Moult, Glass Tech. **23** 106-112 (1982).
9. D.B. Spalding, Int. J. Num. Meth. Eng. **4**, 551-573 (1972).
10. R.J. Adrian, C.S. Yao, Appl. Opt. **24**, 44-52 (1985).
11. R.J. Adrian, A. Rev. Fluid Mech. **23**, 121-132 (1991).
12. P. Mills, P. Snabre, Europhys. Lett. **25**, 651-656 (1994).
13. F. Yamamoto, Y. Dai, M. Koukawa, M. Itoh, T. Uemura, *Numerical simulation on error analysis in particle tracking velocimeter by correlation method*, in: flow visualization, ASME **85**, 9-14 (1989).
14. Y.A. Hassan, T.K. Blanchat, C.H. Seeley Jr, R.E. Canaan, Int. J. Multiphase Flow **18**, 371-395 (1992).